Experimental Mechanics (2008) 48:139–152
DOI 10.1007/s11340-007-9118-9

An Experimental Investigation into the Acoustic Characteristics of Fluid-filled Porous Structures—A Simplified Model of the Human Skull Cancellous Structure

A.K. Ghosh · A.D. Williams · J.M. Zucker · J.L. Mathews · N. Spinhirne

Received: 25 July 2006 / Accepted: 26 December 2007 / Published online: 20 February 2008

Abstract In nature, shape and structure evolve from the struggle for better performance. Often, biological structures combine multiple beneficial properties, making research into mimicking them very complex. Presented here is a summary of observations from a series of experiments performed on a material that closely resembles the human skull bone's cancellous structure under acoustic loads. Transmission loss through flat and curved open-cell polyurethane foam samples is observed using air and water as the two interstitial fluids. Reduction in strength and stiffness caused by porosity can be recovered partially by filling the interstitial pores with a fluid. The test findings demonstrate the influence of the interstitial fluid on the mechanical characteristics of a porous structure in a quantitative manner. It is also demonstrated that the transmission loss does not depend only on the mass per unit area of the structure as predicted by acoustic mass law. Current tests also demonstrate that the transmission loss is more sensitive to the interstitial fluid than the shape and support conditions of the structures. Test observations thus support the concepts of "moisture-sensitivity of biological design" and the "law of hierarchy in natural design".

Keywords Acoustic · Fluid-filled · Porous · Skull · Cancellous

A.K. Ghosh (✉, SEM member) · J.L. Mathews
Mechanical Engineering, New Mexico Tech,
Socorro, NM 87801, USA
e-mail: ashok@nmt.edu

A.D. Williams
Air Force Research Laboratory, Space Vehicle Directorate,
Kirtland AFB, NM 87117, USA

J.M. Zucker
High Explosive Physics Team, Los Alamos National Laboratory,
Los Alamos, NM 87545, USA

N. Spinhirne
Materials Engineering, New Mexico Tech,
Socorro, NM 87801, USA

Introduction

In nature, shape and structure evolve from the struggle for better performance. Often, biological structures combine multiple beneficial properties, making research into mimicking them advantageous. Presented here is a summary of observations from a series of experiments performed on a material that closely resembles the human skull bone's cancellous structure under acoustic loads.

Significant progress has been made recently in understanding natural systems through advances in medical science such as 3D Doppler echo, MRI image reconstruction techniques, and computer simulation methods. It is observed that normal skull bone has a dense outer shell (cortical bone) enclosing a central porous region (cancellous bone or trabecular bone) with fluid in the interstitial pores. Cancellous bone structure is a functionally graded structure that is less dense, open-celled, and rod-like where stress is low and transitions to a closed, shell-like structure at locations of higher stresses. Wolff [1] observed that the architecture of trabecular bone follows the principal stress trajectories. This observation has been supported by numerous studies [2–4] on femoral head and neck bone structures. Recently, Gefen and Seliktar [5] have demon-

strated that the trabeculae do not necessarily align at right angles as hypothesized by Wolff.

There is plenty of literature dealing with the study of human skull (*in vivo*, bony part only) as a structural shell of which some have accounted for the dynamic environment. Fry and Barger [6] measured the acoustical properties (scattering, transmission loss and reflection) of human skull in the frequency range of 0.25–2.2 MHz. Samples studied were relatively large sections of human skull including adult, child and infant subjects. They demonstrated that the dense, outer shell acts more like a reflector and allows minimal transmission inward. Energy that is transmitted inward is primarily absorbed by the porous middle layer. In addition to the structural studies of bone, there has been a series of annual bone fluid-flow workshops since the early 1990s. Most of the work has concentrated in the fluidic contribution to the growth and maintenance of bones, including bone remodeling and bone repair [7–9]. There has been some focus on transport related to the supply of nutrients, the movement of macromolecules and cells, and the removal of wastes. In addition, work exists on the mechanical interaction of fluid and solid phases. It is aimed at revealing how stress on the structure leads to convection of interstitial fluid thus enhancing transport of the nutrients. Some of the work on remodeling pays special attention to the role of fluids. Here the right kind of solid mechanical stress leads to the remodeling of bone structure to better deal with future stress. Fluids have several roles besides transport, including passing signals, pressure distribution, and protection. This relationship has not been conclusively studied.

Bone is composed of 25% fluid by weight with the reminder composed of organic and mineral components configured hierarchically to allow for dynamic optimization of the structure for function, Knothe Tate [10]. The health of bone depends on the ability of the system to recognize and respond to mechanical, electrical, and chemical stimuli providing the basis for adaptation. The interaction between the solid and fluid phases of bone underlies much of its mechanical properties (e.g. energy absorption, viscoelastic damping, and elasticity). Although these flow regimes are important, the objective of this paper is to demonstrate the influence of fluid in the interstitial pores of a manufactured cellular material (simplified model of skull structure) under acoustic loading. The exact biochemical composition and viscosity of this bone fluid is unknown because of the practical difficulties of obtaining a sample size sufficiently large for analysis. Hence, bone fluid is often idealized as a fluid with characteristics between blood plasma and lymph fluid, Aukland [11]. Conceptually, bone fluid serves as a coupling medium through which energy is transferred from the system to the cells that have the machinery to remodel the tissue, thereby providing an elegant feedback mechanism for functional adaptation.

Under mechanical stress, bone behaves much like wood. Figure 1 shows the stress-strain behavior of cancellous bone at two different relative densities and wood at one density. Features of this stress-strain behavior are: (1) at small strains the behavior is linear-elastic, (2) beyond the linear-elastic regime, there is a long stress plateau followed by a steep rise in stress. Gibson and Ashby [12] have extensively studied the loading of cellular material including bone and timber. They demonstrated that the change in the stress-strain behavior caused by variation in relative density was similar for both materials [12]. As the relative density of wood increases, the rate of increase in Young's modulus in the radial direction and tangential direction increase three times faster than that in the axial direction. The Young's modulus in the axial direction is much larger than in the tangential direction and radial direction, which are roughly equal [12].

The stress-strain behavior of many artificial cellular materials, such as foams, used in energy absorption

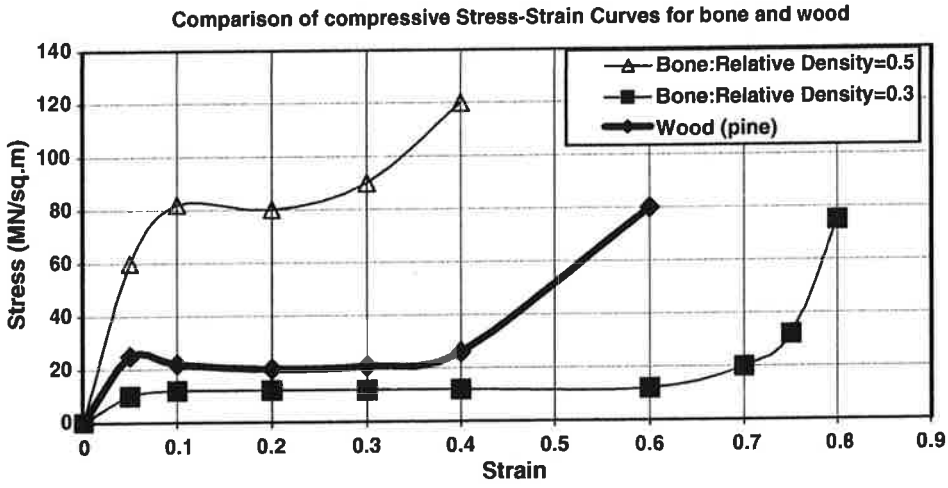

Fig. 1 Stress-strain behavior of cancellous bone and wood

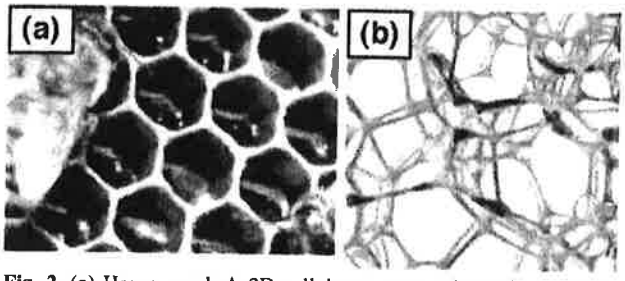

Fig. 2 (a) Honey comb-A 2D cellular structure with ends open; (b) 3D open structure

products like acoustic blankets, packaging materials, and crush padding are similar. Foams are formed typically by generating bubbles in a liquid medium. After nucleation, the bubbles grow and pack together. When bubbles are in contact, a flat surface defines the boundary between two neighboring bubbles forming polyhedral cells. The bubbles are then solidified resulting in a cellular solid or foam. When the faces of the polyhedra remain intact the foam is classified as closed-cell. If the cell walls are broken and only the cell edges remain intact, the resulting structure is open-cell foam. Figure 2(a) shows a 2-dimensional (D) porous structure of natural origin and Fig. 2(b) a man-made 3D open celled foam structure.

The relative density of a cellular solid is the ratio of the density of the cellular material to the density of the solid from which the cell walls are made, The value can be as low as 0.002. Almost any material can be foamed; however, polymers are the most common. Figure 3 shows the variation of mechanical characteristics between the solid and porous states of a material [12].

Biot's theory [13] of poroelastic solids describes the behavior of interstitial fluids in porous media and provides the biophysical basis for load-induced fluid flow in bone. According to his theory, compression deforms the solid matrix of a porous media instantaneously increasing the pressure of the fluid within the pores. Disparate pressures between the interior and exterior of a porous solid cause a net flow of the fluid. Fluid flows out of the porous solid causing the solid matrix around the pores to relax. Associated with matrix relaxation around the pores, the fluid pressure within the pores decreases until it equilibrates with the surface pressure of the solid. Removing the load reverses the pressure gradient and the fluid flows back into the sample's area that was compressed until equilibrium is again reached. The rate of pressure reduction during matrix relaxation is an exponential decay function dependent on the poroelastic behavior of the material.

Bassett [14] was one of the first to describe the concept of mechanical load-induced fluid flow in bone. Piekarski et al. [15] have developed analytical, as well as numerical models to simulate the fluid flow phenomena in an idealized system of a bone tissue network. The existence of mechanical load-induced fluid flow has been proved recently through visualization of fluid displacements induced through controlled mechanical loading of cortical and trabecular bone, Knothe Tate et al. [16].

Fluid flow through an open-cell foam usually contributes to the elastic moduli if the fluid has a high viscosity or if the strain-rate is exceptionally high, Tyler et al. [17]. Cell fluids contribute to the strength of open cell foams in a completely different way. There are a number of ways to analyze this. The simplest is to treat the foam as a porous medium characterized by an absolute permeability, (K), and the flow through it is described by Darcy's law. The contribution of viscous flow to foam strength can be given as:

$$\sigma_g = \frac{C\mu\varepsilon^*}{1-\varepsilon}\left(\frac{L}{l}\right)^2 \tag{1}$$

Where σ_g is the contribution of a viscous fluid to the strength; C is the constant of proportionality; μ is the viscosity of the fluid; ε^* is the strain-rate; ε is the strain; L is the length of a block of foam and l is the cell-edge length.

Reductions in strength and stiffness caused by porosity, as displayed in Fig. 3, can be recovered by filling the interstitial pores with fluid. The relation between the porosity and the corresponding strength loss and making

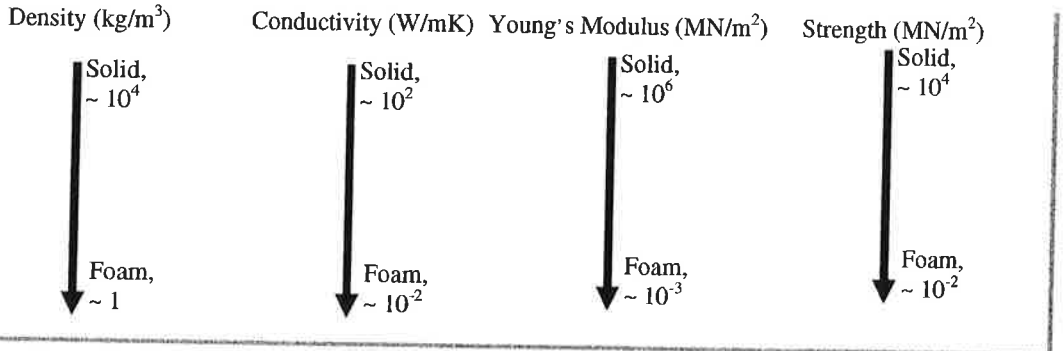

Fig. 3 Variation of properties due to foaming

up of this loss by adding fluid is not established. The long-term goal of the current study is to establish these relationships in quantitative terms. Many previous researchers have hypothesized mechanical coupling between the solid and fluid phases, but there is little documentation that demonstrates conclusively the influence of the interstitial fluid on the mechanical characteristics of a porous structure in a quantitative manner. The current test program is aimed to fill this gap.

Objective

The objective of this effort is to determine quantitatively the mechanical coupling between the interstitial fluid and porous solid in Natural/Biological Design rules.

Experimental Investigation

Tests described in this paper demonstrate the influence of interstitial fluid on the characteristics of human skull cancellous bone structure. Because of the skull's complex structure, experimental and computational investigations are performed using commercially available porous structure that best resembles skull's cancellous structure. Selection of the material is performed on the basis of following criteria:

1. Open cell cellular material;
2. Porosity of around 80%;
3. Deformable and high resiliency.

After a thorough review process, quick recovery open-cell polyurethane foam (PUF) with the following characteristics is selected. The stress-strain behavior of the PUF (rating 4) is given in Fig. 4. Comparison between Fig. 1 and Fig. 4 demonstrate that PUF does not have the long stress plateau as seen with natural structures followed by a steep rise in the stress with the stress-strain curves. However, the other properties are similar.

- Density=240 kg/m^3 (15 pcf);
- Tensile strengths
  a) Rating 2 [0.14 MPa (20 psi)]
  b) Rating 4 [0.28 MPa (40 psi)] and
  c) Rating 8 [0.56 Mpa (80 psi)];
- Young's Modulus=0.1 GPa;
- Thickness=6.34 mm (1/4″), 4.76 mm (3/16″), 9.53 mm (3/8″) and 12.7 mm (1/2″).
- Porosity=~ 80%

Porosity

Three samples for each thickness are cut and weighed using a triple-beam balance. The samples are then fully soaked, surface dried, and re-weighed. From these values, the porosity is calculated to be approximately 80%. To verify the accuracy of the measurement and the consistency of the material a large 12″×12″ plate is tested, and the variance between the samples is calculated to be 2%.

Foam Structure

This part of the study focuses on determining the characteristics of the foam such as pore sizes, distribution, and cell morphology to provide information for the material modeling. Tests include (1) Optical Microscopy of the fluid filled samples, and (2) Field Emission Scanning Electron Microscopy (FESEM) to obtain microstructure.

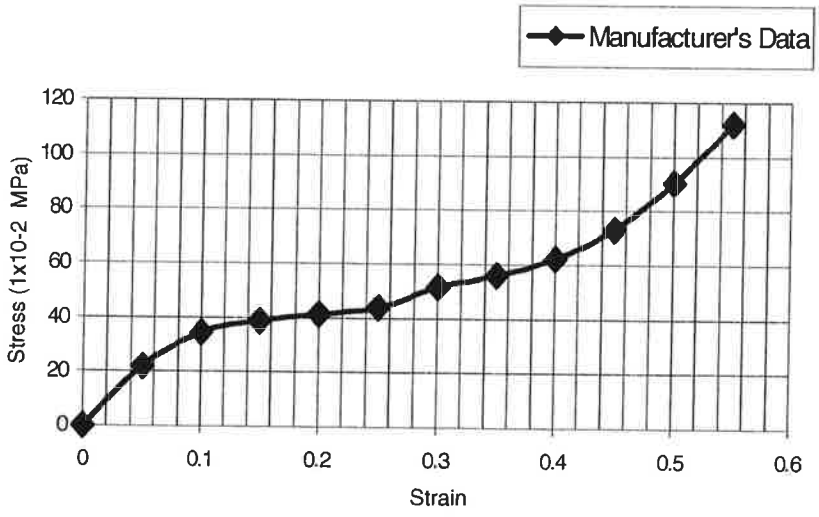

Fig. 4 Stress-strain behavior of the quick recovery polyurethane foam

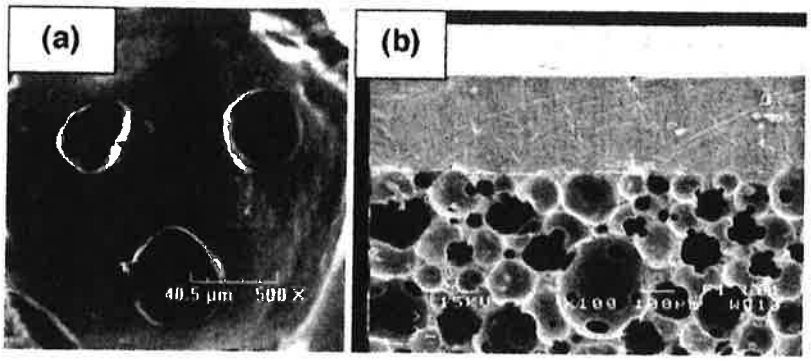

Fig. 5 (a) Magnified view of a single cell of the polyurethane foam (magnification 500); (b) Interface between the foam and the sealant layer (magnification 100)

Figure 5(a) shows a single cell of the PUF (magnification 500) and Fig. 5(b) shows the interface between the foam and the sealant layer (magnification 100). Pore size ranges between 50–200 µm.

Selection of Sealant

To properly test the fluid filed samples (FFS), the water is contained within the foam by coating all six-boundary surfaces with water sealant. Ideally, the sealant should (1) adhere well to wet surfaces and (2) have minimal influence on the characteristics of the plate. Four different marine grade sealants, (clear sealant, blue RTV i.e., room temperature vulcanizing silicone, black RTV silicone, and the less corrosive ultra blue silicone) are considered. The blue RTV silicone is selected because it is translucent, and it is easy to determine the thickness.

Acoustics Characteristics

An important acoustic characteristic of the human skull is its attenuation of acoustic energy. Soft porous materials absorb incident, airborne, sound waves converting them into heat. When fluid-filled systems (FFSs) are exposed to acoustic loads, two mechanisms become responsible for the absorption of the acoustic energy:

(a) Viscous flow losses: When a structure with interconnected pores filled with compatible fluid is loaded, relative motion between the fluid and the surrounding structure results in boundary-layer losses.
(b) Internal Friction: Under acoustic loading, the porous structure will compress or flex, causing internal friction.

To achieve greater attenuation increasing the deformation of the system is important. Attenuation can also be improved by developing shear stresses throughout the materials transport channels. The individual contribution of each will depend on many parameters. Some of these parameters include: (1) characteristics of the porous structure, (2) characteristics of the fluid in the interstitial pores, and (3) characteristics of the load.

Sound transmission loss through a media is defined as the ratio between incident sound power (P_{in}) and transmitted sound power (P_{tr}) expressed in decibels (dB) [18].

$$TL = 10\log_{10}\left(\frac{P_{in}}{P_{tr}}\right) \tag{2}$$

The transmission loss is also dependent on the incidence angle φ, as defined in Fig. 6. Additionally, the transmission loss through a plate is greatly reduced when exposed to its coincidence frequency, which is defined as

$$f_c = \frac{c^2}{2\pi}\sqrt{\frac{m}{D}} \tag{3}$$

Where c is the propagation velocity of incident sound waves, m is the mass of the panel per unit surface area, and D is the plate bending stiffness as defined in equation (4).

$$D = \frac{Et^3}{12(1-\nu^2)} \tag{4}$$

Where E is the Young's modulus, t is the panel thickness; ν is the Poisson's ratio.

Below the coincidence frequency, the mass law characterizes the transmission loss because this region is dominated by the mass of the plate [18].

$$TL(\varphi) \approx 20\log_{10}\left(\frac{\omega m\cos\varphi}{2\rho c}\right) \tag{5}$$

Where ω is the fundamental frequency and ρ is the mass density of the material.

Above the coincidence frequency the transmission loss is dominated by damping at the coincidence frequency and by

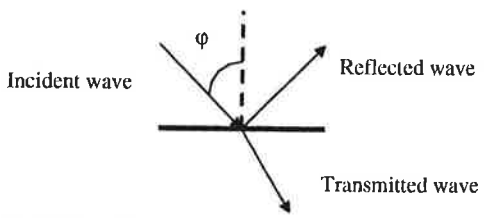

Fig. 6 Definition of incident angle

the bending stiffness of the plate. In the current study, the coincidence frequencies of the samples are much greater than the highest tested frequency.

Experimental Investigation

Two sets of tests are performed in a 6-month interval using samples prepared by two separate groups of students following the same procedures and using the same commercial polyurethane foam.

- SET 1: 12 flat-samples with characteristics as given in Table 1.
- SET 2: 6 samples (2-flat and 4-domed) with characteristics as given in Table 1.

Preparation of samples

Both dry (air filled) and fluid-filled (FF) samples are prepared in the same manner. The water-filled samples are prepared by submerging the foam while a heavy steel cylinder is slowly rolled over the foam. The steel cylinder is heavy enough to compress the foam forcing air out of the foam, which is replaced by water once the pressure is removed. Both dry and fluid-filled samples are sealed with Lexel™, to reduce transmission loss variability associated with the sealant.

Experimental setup

All samples are tested using a custom-made acoustic transmission loss (TL) tube located at the Air Force Research Laboratory, Space Vehicle Directorate (AFRL/RV) on Kirtland Air Force Base, Albuquerque, NM. The TL tube method, based on work by Song and Bolton, is an alternative test method to the Reverberation Rooms Method, ASTM E90–04 and the Sound Transmission Loss Suite Method SAE J1400 [19–21]. A schematic representation of the TL tube is presented in Fig. 7 and a picture of the actual tube, constructed in-house at the AFRL/RV, is shown in Fig. 8. The TL tube is constructed using 6″ diameter schedule 80 PVC pipe that is embedded in a 2″ thick layer of concrete to avoid losses through the walls. The test sample is located between the two sections of the tube (the source tube and the receiving tube) and is acoustically excited using a 6″ loudspeaker. Four microphones (1, 2, 3, and 4 in Fig. 7) are used to measure the sound pressure levels on both sides of the sample. The upstream microphones are used to determine the incoming and reflected plane waves. The downstream microphones are used to determine the absorbed and transmitted portions. Because there are four variables but only two equations to solve, two different boundary conditions were used for each sample: one consisted of an open receiving tube end and the other consisted of an anechoic termination. The normal incident absorption coefficient for the anechoic termination is

Table 1 Material characteristics of the test samples

Set no.	Sample no.	Shape Flat/Dome	Fluid/air filled	Thickness mm (in)	Foam rating	Density (kg/m3)	Mass per unit area (kg/m2)	Difference in mass/area between dry and wet samples
SET 1	1	Flat	Air	6.35 (1/4)	2	265	1.68	
	2	Flat	Fluid	6.35 (1/4)	2	777	4.93	3.25
	3	Flat	Air	6.35 (1/4)	4	234	1.49	
	4	Flat	Fluid	6.35 (1/4)	4	1001	6.36	4.87
	5	Flat	Air	6.35 (1/4)	8	232	1.47	
	6	Flat	Fluid	6.35 (1/4)	8	1000	6.35	4.88
	7	Flat	Air	4.76 (3/16)	2	273	1.30	
	8	Flat	Fluid	4.76 (3/16)	2	1048	4.99	3.69
	9	Flat	Air	9.53 (3/8)	2	248	2.36	
	10	Flat	Fluid	9.53 (3/8)	2	1015	9.67	7.31
	11	Flat	Air	12.70 (1/2)	2	253	3.21	
	12	Flat	Fluid	12.70 (1/2)	2	1024	13.00	9.79
SET 2	13	Flat	Air	12.70 (1/2)	4	284	3.61	
	14	Flat	Fluid	12.70 (1/2)	4	765	9.72	6.11
	15	Dome	Air	12.70 (1/2)	4	300	3.81	
	16	Dome	Fluid	12.70 (1/2)	4	865	10.99	
	17	Dome	Fluid	12.70 (1/2)	4	877	11.14	
	18	Dome	Air	12.70 (1/2)	4	310	3.94	Average = 7.19

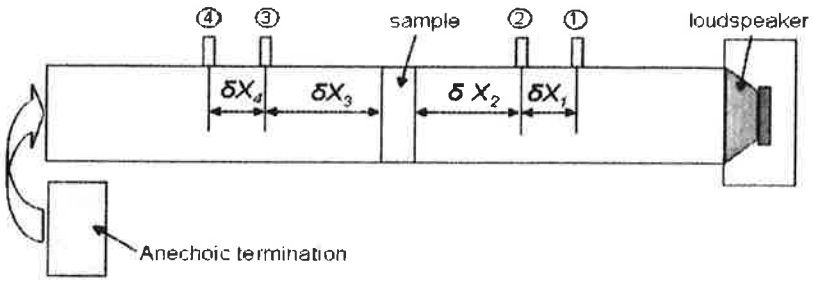

Fig. 7 Schematics of the transmission loss (TL) tube

measured at 0.97 in a two-microphone standing wave tube using ASTM standard C 384 [22]. A SigLab data acquisition system is used for signal processing.

Experimental procedure

For these experiments, acoustic excitation consisting of white noise from 250 to 1000 Hz is produced with the loudspeaker. Microphone spectra are recorded with SigLab, and the TL is calculated based on the following procedure. Figure 9 presents the concept used for TL computation. Broadband sound waves generated by the loudspeaker propagate down the tube as a plane wave. Upon impinging on the sample face part of the wave is reflected back, part of it is absorbed by the sample, and part of it is transmitted through the sample. On each face of the sample, there is an incident and a reflected wave with amplitudes A and B, respectively.

Based on the scheme presented in Fig. 9, one can write the following system of equations (6) in terms of wave amplitudes where α, β, γ, and δ, are parameters dependent on frequency ω.

$$\begin{Bmatrix} A_1(\omega) \\ B_1(\omega) \end{Bmatrix} = \begin{Bmatrix} \alpha(\omega) & \beta(\omega) \\ \gamma(\omega) & \delta(\omega) \end{Bmatrix} \begin{Bmatrix} A_2(\omega) \\ B_2(\omega) \end{Bmatrix} \tag{6}$$

Transmission Loss, TL (dB), is defined as: ten times the common logarithm of the ratio of the airborne sound power incident on the partition to the sound power transmitted by the partition and radiated on the other side [23]. It is calculated as:

$$TL(\omega) = 20 \log_{10} |\alpha(\omega)| \tag{7}$$

The coefficient, $\alpha(\omega)$ in equation (7) is calculated from the cross-spectra measurements taken with SigLab for the two termination boundary conditions.

For the anechoic termination, different types of foam are necessary since just one type of material is not sufficient to absorb every frequency used during testing. The panels are tested for frequencies between 250 and 1000 Hz. For circular tubes the upper frequency is dependent on the

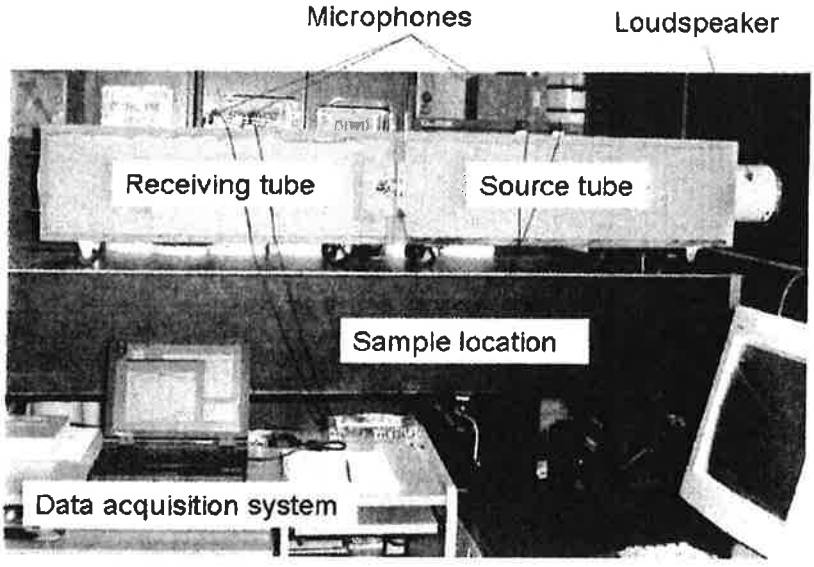

Fig. 8 Transmission loss tube experimental setup

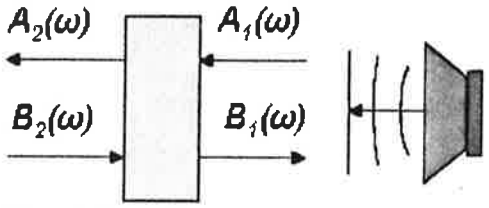

Fig. 9 Wave partition on the sample face

diameter. At frequencies above this range the incident and reflected waves are not likely to be planar because of cross modes in the tube. The tubes are pressed to the walls of the panel through Plexiglas end covers. These covers are drawn tight by an aluminum hub surrounding the end covers and the specimen. The aluminum hubs also serve to reduce sound losses at the joint by providing a high impedance mismatch to the interior panel and the surrounding atmosphere. A loudspeaker is used to generate a plane wave field in a standing wave tube and a single microphone is used to measure the transfer functions between the signal provided to the loudspeaker and the sound pressure at the four locations as shown in Fig. 7.

Observations and discussion for SET 1 samples

The plot of transmission loss versus frequency for all samples under SET 1 is shown in Fig. 10. In the legend, Plate_1/4_r=2_a signifies a plate sample of 1/4″ thickness made with rating 2 grade polyurethane foam where pores are filled with air i.e. as manufactured. The highest TL of approximately 40 dB is observed for the 1/2″ plate sample with fluid filled pores. It is observed that the higher the mass per unit area of a sample, the higher its TL value. This plot supports the acoustic mass law, which states that the TL of a material is proportional to its mass per unit area and not mass per unit volume i.e. mass-density (refer to Table 1). All of the fluid filled samples demonstrated higher TL than the air filled samples.

Figure 11 is obtained from Fig. 10 taking the difference between the fluid filled samples and air filled samples. This plot gives the contribution of the interstitial fluid on the transmission loss for samples of different thickness and rating. The highest difference of 11 dB is found for the 1/2″ plate at around 400 Hz. This difference quickly decreases with the increase in frequency. All but the 3/16″ samples show similar characteristics. The influence of the interstitial pore-fluid on the TL does not show any dependence on the frequency for the Plate_3/16_r=2 case with the difference in mass per unit area equal to 3.69 kg/m^2, which is much smaller than the difference of most of the other plates as given in the legend box in Fig 11. The rate of increase in the TL value is not directly proportional to the rate of increase in the mass per unit area.

Observation and discussion for SET 2 samples

The first test under SET 2 consists of two samples i.e. samples 13 and 14. The objective of this test is to demonstrate the repeatability of the test process. The plots of transmission loss versus frequency for these two samples are shown in Fig. 12. The highest value of TL for the dry sample is found to be approximately 32 dB, which is very close to the value found during SET 1 tests. The TL for sample 14 is found to be somewhat less when compared to

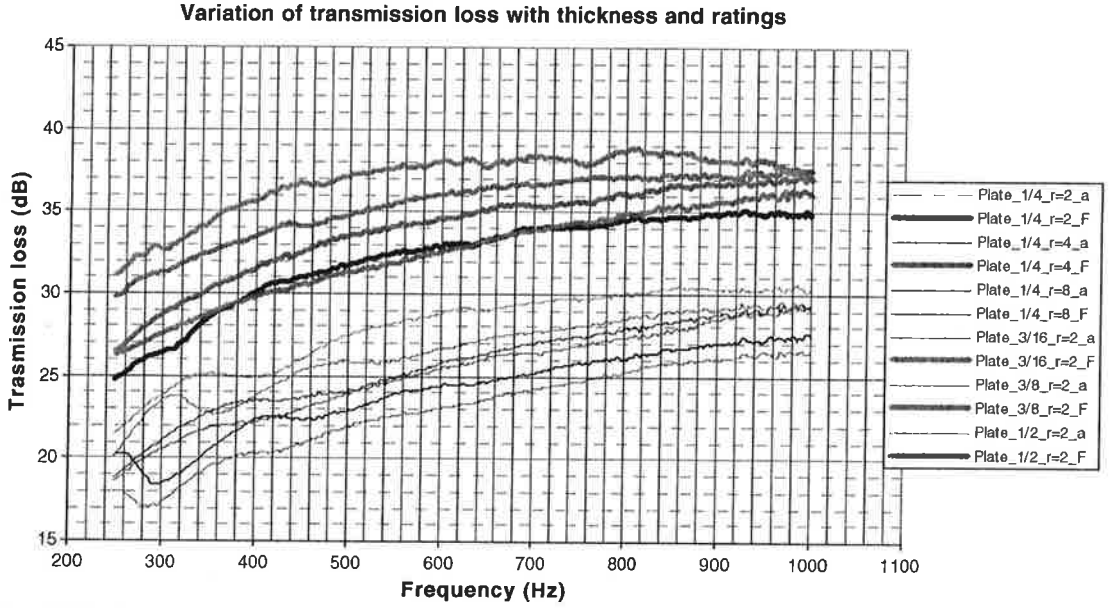

Fig. 10 Transmission loss versus frequency

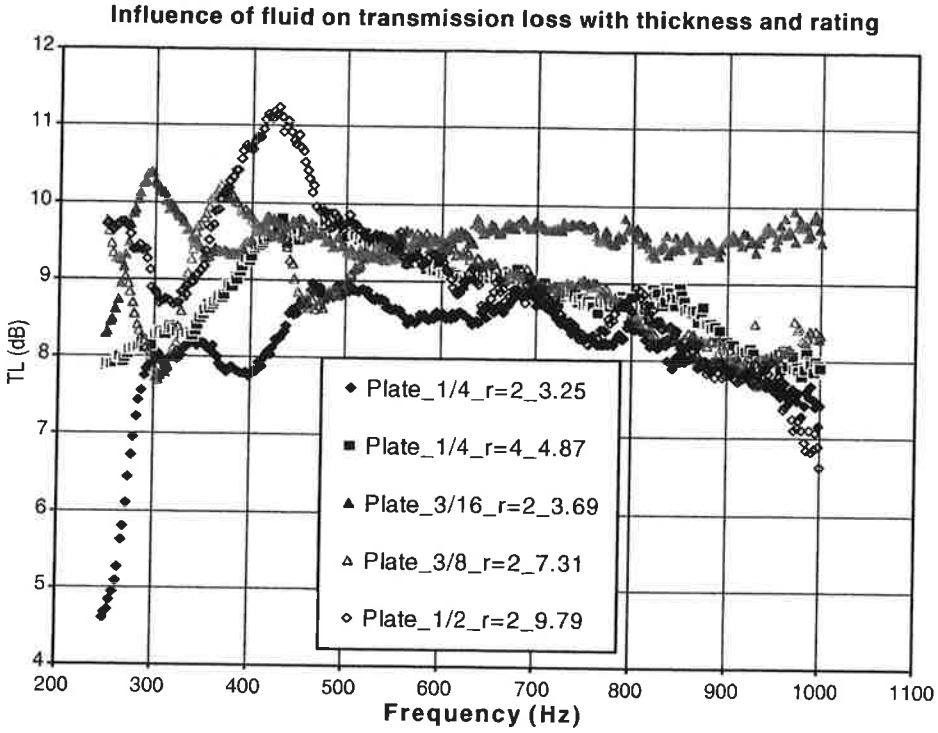

Fig. 11 Influence of the fluid on the transmission loss

similar value from SET 1. However, there exists no sample in SET 1 that has the same rating and thickness as that of sample 14 in SET 2.

After demonstrating repeatability, the next round of tests are carried out using four samples. In this round, both the geometry of the samples and the support conditions are varied and the influence of moisture in the interstitial pores is investigated. Experimental observations are plotted in Figs. 13 and 14. The data for the two dry domed samples and the two wet domed samples are averaged and then plotted in Fig. 13. Also plotted in Fig. 13 is the mass law [equation (5)] for the dry and wet samples. The mass law is not applicable for nonhomogenous materials such as current samples. They are

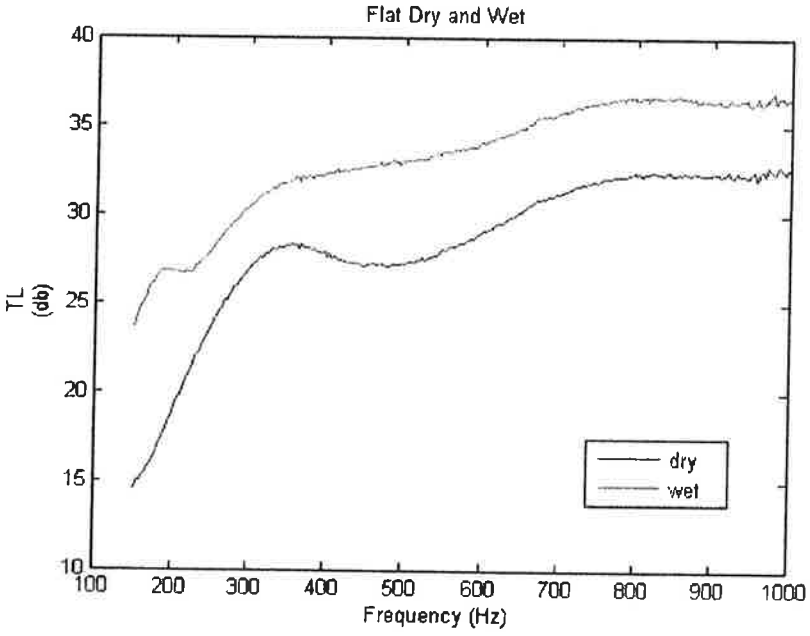

Fig. 12 Transmission loss versus frequency (repeat tests). Data below 250 Hz is not valid

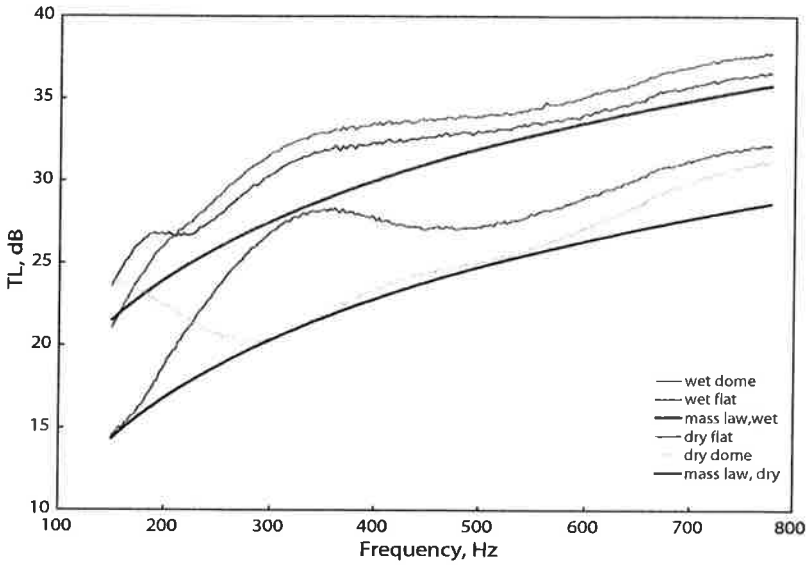

Fig. 13 TL vs Frequency for samples and mass law (flat and domed sample). Data below 250 Hz is not valid

presented here for reference purpose only. In agreement with the mass law, the transmission loss through the flat wet plate is found to be greater than that of the dry flat plate. Above 300 Hz, the difference in average transmission loss between the wet and dry plates vary between 5–8 dB.

Although the wet sample also has a drop in transmission loss at around 500 Hz, it is minimal, but it does have a noticeable dip around 250 Hz. The transmission loss dip in the wet sample occurs over a narrower range of frequencies compared to the dry sample. When the flat wet plate is compared with the wet dome the difference in transmission loss is minimal. The difference in transmission loss is approximately 1 dB from 250 to 775 Hz. Most likely this is caused by the lack of curvature in the wet samples.

The differences between the flat dry sample and the domed dry samples are the most dramatic of all the results. At frequencies above 250 Hz, the flat sample had a greater transmission loss. The differences in transmission loss are significant from 275 to 450 Hz.

The domed samples also have a dip in the transmission loss that corresponds to the flat sample, but it is more pronounced and occurs at a lower frequency. The decrease in transmission loss is characteristic of an edge-constrained porous foam and occurs when the foam resonates against the constraint [24]. It is also observed that the frequency at which the dip in transmission loss occurs is dependent on the foam's solid phase stiffness [24]. This may explain why the pronounced dip is only seen in the dry dome samples. In the other samples the dip most likely occurs around 100 Hz, which is below the lowest frequency tested. After 350 Hz, the transmission loss levels out and then rises again. These experimental trends correspond well to previous finite element models [24].

The dome samples are tested in both the convex and concave directions as defined earlier and the results are shown in Fig. 14. In both the wet and dry samples, there is little difference between the convex and concave orientations. In the dry sample, the concave transmission loss is slightly greater than the convex orientation at frequencies between 250–300 Hz. Above 300 Hz, the two tests were nearly identical. The results are similar for the wet samples; the concave orientation has slightly greater transmission loss at frequencies between 250–300 Hz, above which the transmission loss is nearly identical.

Model Development

An initial attempt to create a model using acoustic attenuation theory in solids to fit experimental data is provided in this section. The samples are considered to be homogenous solids, and values for the unknown constants are found empirically. The simple model presented here excludes some of the pertinent physics and characteristics but provides good initial results.

A sound wave with initial pressure, P_0, experiences exponential attenuation as it travels through a medium. The energy dissipated per unit time can be given by

$$\text{Energy dissipated per unit time} = \frac{P_0^2 \alpha \delta \chi}{\rho c} \exp[-2\alpha\chi] \quad (8)$$

where α is the attenuation coefficient, ρ is the density of the medium, c is the propagation velocity, and δx is the length of the sample [25].

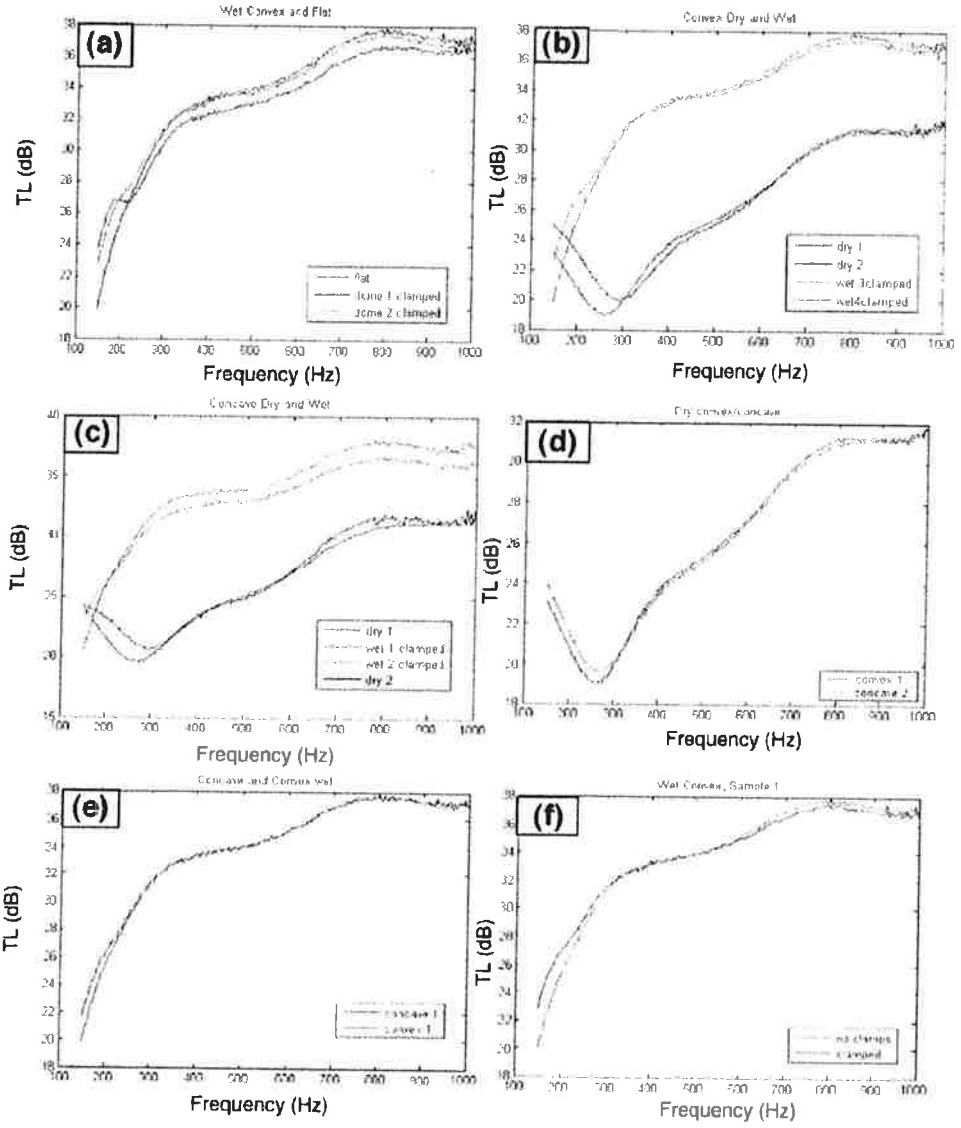

Fig. 14 (a–f) Influence of fluid on TL for samples with different shape and edge condition. Data below 250 Hz is not valid

Taking P_{in} equal to equation (8) at $x=0$, and P_{tr} equal to equation (8) at $x=\delta x$, equation (2) becomes:

$$TL = 10Log\left[\exp\left(2\alpha\delta x\right)\right] \tag{9}$$

The attenuation coefficient is dependent on the frequency of the acoustic wave and can be sufficiently modeled by a power law as given in equation (10)

$$\alpha = \alpha_0\omega^{\gamma} \tag{10}$$

where α_0 is the attenuation constant, ω is the frequency, and γ is between 0 and 2 for most materials.

This power law works for a varicty of media, including liquids and porous media [26]. Unfortunately, α_0 and γ are determined empirically in this case. Further complicating matters is the dependence between α and the level of porosity [27]. Substituting equation (10) into equation (9) yields

$$TL(\omega) = 10Log\left[\exp\left(2\delta x\alpha_0\omega^{\gamma}\right)\right] \tag{11}$$

Equation (11) provides an initial predictor for transmission loss based on frequency and two empirical constants. This model will predict the loss through the sample. However, it does not account for the resonance issues associated with edge effects, and it requires the assumption that the acoustic wave is normal to the sample.

Model optimization

The model was optimized to a 1/4 in sample. The unknown constants, α_0 and γ, are varied until the desired shape and

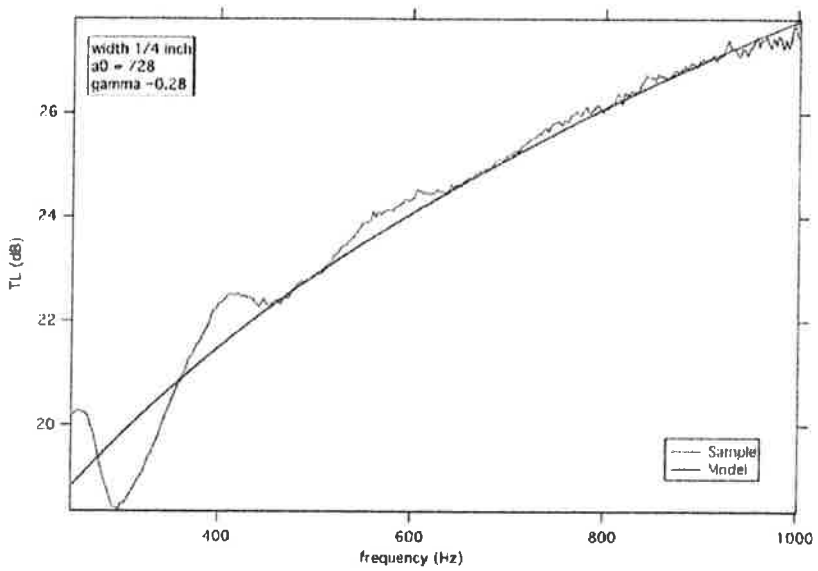

Fig. 15 The optimized model

position of the transmission loss versus frequency plot is achieved. A plot of the optimized curve and the experimental data is given in Fig. 15. The values obtained are: α_0=728 and γ=0.28.

From Fig. 15, two failures are apparent. One is that lack of any resonance in the model, and the other is the curvature at high frequencies. At frequencies greater that 1,000 Hz, the model would climb faster than the experimental data.

Model validation

The model is compared to the results for three samples; 3/16 inch (sample 5), 3/8 inch (sample 7), and 1/2 inch (sample 9). The results are show in Figs. 16, 17, and 18. The predictive capabilities of model are adequate for a first order model.

The model under predicts the TL for the 3/16 inch sample, but then over predicts for the 3/8 and 1/2 in samples. Furthermore, as sample width increases, the predicted curvature seems to become more inaccurate. This means that the model has a great dependence on sample width.

Conclusions

Experiments are performed to determine the influence of interstitial fluid on acoustic characteristics of flat and curved

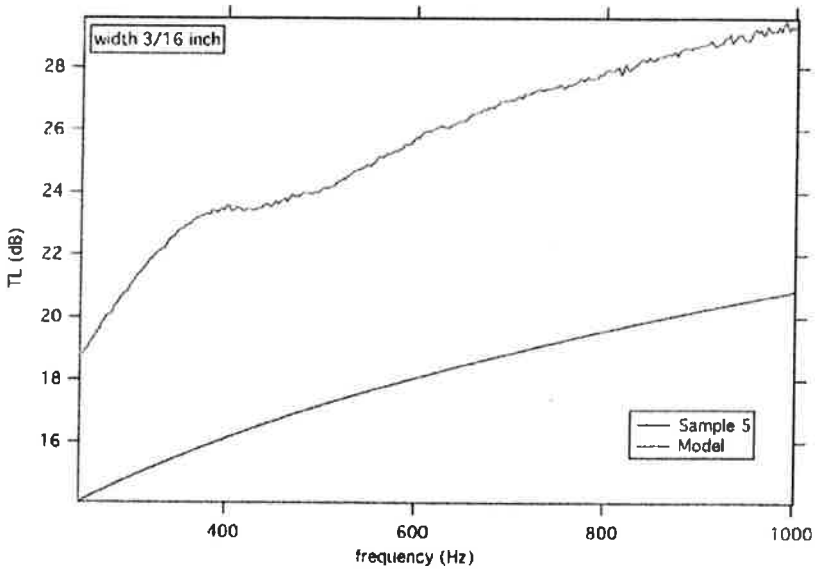

Fig. 16 Comparison of the model with experiment (3/16 inch sample)

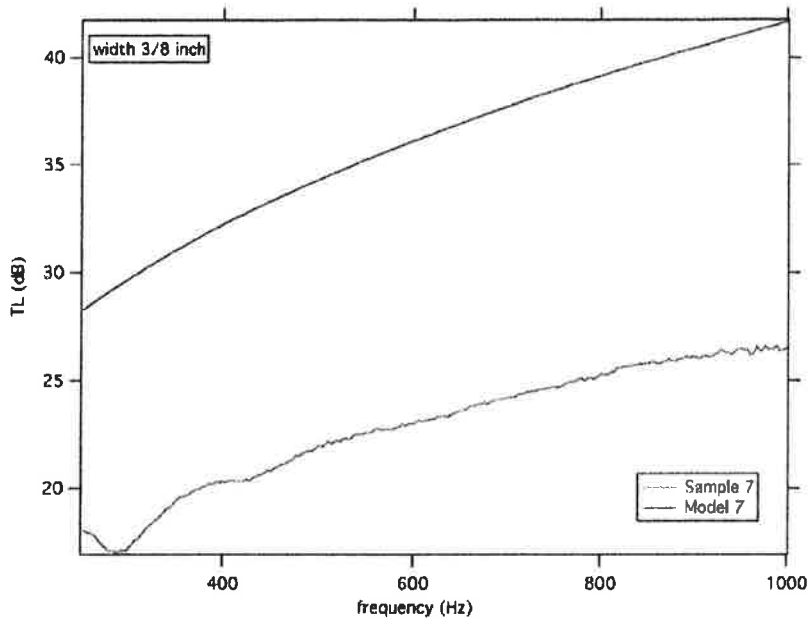

Fig. 17 Comparison of the model with experiment (3/8 inch sample)

polyurethane samples that resembles skull structure. The experiment yields the following conclusions:

Sample 12 with the highest mass per unit area demonstrated the highest TL (refer Fig. 10) as predicted by the acoustic mass law. But the rate of increase in TL due to interstitial fluid is not directly proportional to the rate of increase in mass per unit area. The sample with 3/16 in thickness yielded highest change in TL. The same sample demonstrated near constant TL throughout the frequency range of the current test program. This demonstrates the coupling between the solid and fluid phases in a quantitative manner.

Domical samples, both convex and concave, can cause comparable transmission loss. Although the difference between fluid-filled-flat-samples and fluid-filled-domical-samples was minimal, there were significant differences between the air-filled-flat-samples and air-filled-dome-samples. This observation supports the concepts of "moisture-sensitivity of biological design" and the "law of hierarchy in natural design". The process of optimization of skull structure at the macro level can be achieved at two stages: (1) the first stage of optimization is accomplished through shape i.e. turning from flat to curved, thereby improving [around 2–5 dB, refer Fig. 13

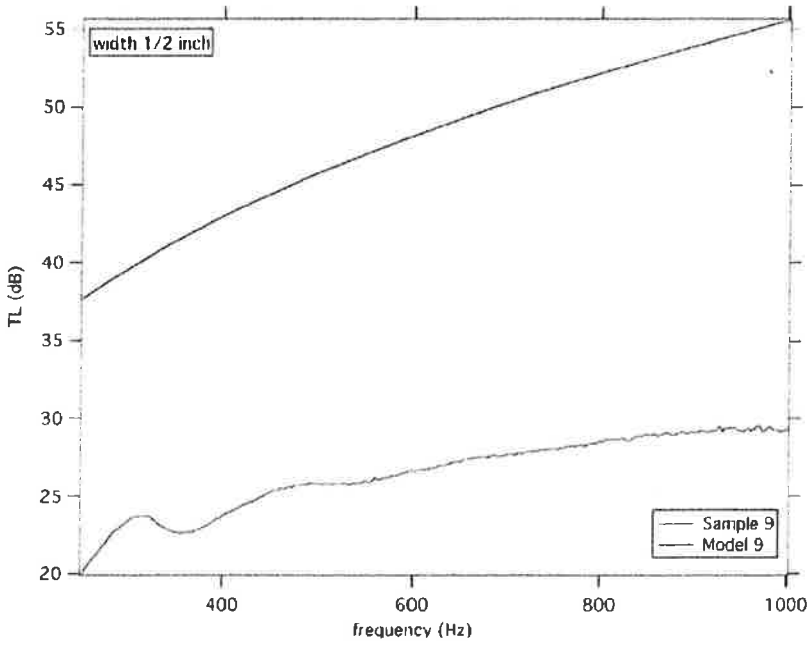

Fig. 18 Comparison of the model with experiment (1/2 inch sample)

and Fig. 14(a)] on transmission loss, and (2) the next stage of optimization is achieved through saturating the interstitial pores with fluid. In this test program water is used with 1/2" thick plate. During this stage, there is considerable improvement. Around 6–8 dB [refer Fig. 14(b), (c)], Figs. 14(d–f) is observed. In addition, it is demonstrated that the fluid filled porous structure is insensitive to change in boundary conditions (i.e. clamped or simply-supported) as well as curvature sign (i.e. convexity or concavity).

In addition to the two afore mentioned major conclusions, the following minor conclusion can be made:

The wet dome samples did not exhibit a dip in transmission loss occurring at 250 Hz like the dry samples. However, both the wet and dry samples dip slightly at 550 Hz and peak at around 700 Hz.

Overall, this is a very early model. It clearly lacks some of the pertinent physics to accurately describe this problem, but it is a good starting point and could lead to a better characterization of acoustical transmission loss for the human skull.

To enhance the model, several factors need to be addressed. The model has no capacity for resonance or edge effects, which is clearly important, nor can it currently account for non-normal incident angles. Additionally, further refinements are needed to include porosity and to improve the α_0 and γ determination process.

References

1. Wolff J (1986) The law of bone remodeling. Springer Verlag, Berlin [English translation from German].
2. Carter DR, Orr TE, Fyhrie DP (1989) Relationships between loading history and femoral cancellous bone architecture. J Biomech 22:231–244.
3. Fyhrie DP, Carter DP (1990) Femoral head apparent density distribution predicted from bone stresses. J Biomech 23:1–10.
4. Rybicki EF, Simonen FA, Weir EB (1972) On mathematical analysis of stress in the human femur. J Biomech 5:203–215.
5. Gefen A, Seliktar R (2004) Comparison of the trabecular architecture and the isostatic stress flow in the human calcaneus. Med Eng Phys 26:119–129.
6. Fry FJ, Barger JE (1978) Acoustical properties of the human skull. J Acoustic Soc Am 635:1576–1590.
7. Montgomery RJ, Sutker BD, Bronk JT, Smith SR, Kelly PJ (1988) Interstitial fluid flow in cortical bone. Microvascular Res 35:295–307.
8. McCarthy ID (1997) Clearance of albumin by cortical bone and marrow. Clin Ortho Related Res 334:24–29.
9. Gatzka C, Knothe U, Niederer P, Schneider E, Knothe Tate ML (1999) A novel ex vivo model for investigation of fluid displacements in bone after endoprosthesis implantation. J Mater Sci Mater Med 10:801–806.
10. Knothe T, Melissa L (2003) Whither flows the fluid in bone?—An Osteocyte's perspective. J Biomech 36:1409–1424.
11. Aukland K (1984) Distribution of body fluids: local mechanisms guarding interstitial fluid. J Physiol (Paris) 79:395–400.
12. Gibson LJ, Ashby MF (1997) Cellular solids—structure and properties. 2nd Edison, Cambridge Uni. Press.
13. Biot MA (1955) Theory of elasticity and consolidation for a porous anisotropic solid. J Appl Phys 26:182–185.
14. Bassett CAL (1968) Biologic significance of piezoelectricity. Calcified Tissue Res 1:252–272.
15. Piekarski K, Munro M (1977) Transport mechanism operating between blood supply and osteocytes in long bones. Nature 269:80–82.
16. Knothe T, Melissa L, Knothe U (2000) An ex-vivo model to study transport processes and fluid flow in loaded bone. J Biomech 33:247–254.
17. Tyler CJ, Ashby MF (1986) Project report. Cambridge University Engineering Department.
18. Krakers LA, Van Tooren MJL, Zaal K, Vermeeren CAJR (2005) Integration of acoustics and mechanics in a stiffened shell fuselage, Part III. Appl Compos Mater 121:21–35.
19. Song BH, Bolton JS (2000) A transfer-matrix approach for estimating the characteristic impedance and wave numbers of limp and rigid porous materials. J Acous Soc Am 107(3):1131–1152.
20. ASTM standard E90–04, "Standard test method for laboratory measurement of airborne sound transmission loss of building partitions and elements".
21. SAE standard J1400, "Laboratory measurement of the airborne sound barrier performance of automotive materials and assemblies".
22. The American Society for Testing and Materials, "Standard test method and impedance and absorption of acoustical materials by the impedance tube method," Annual Book of ASTM Standards 04–06:144–156, C384–C385.
23. ASTM standard CC634–02, "Standard terminology relating to environmental acoustics".
24. Kang YJ, Bolton JS (1996) A finite element model for sound transmission through foam-lined double-panel structures. J Acous Soc Am 99:2755–2765.
25. Kolsky H (1963) Stress waves in solids. Dover Publications Inc., NY.
26. Fellah ZEA, Berger S, Lauriks W, Depollier C (2003) Verification of Kramers-Kronig relationships in porous materials having a rigid frame. J Sound Vibration 120:865–885.
27. Lee KI, Yoon SW (2006) Comparison of acoustic characteristics predicted by Biot's theory and the modified Biot-Attenborough model in cancellous bone. J Biomech 39:364–368.